ϵ-pseudoclassical model for quantum resonances in a cold dilute atomic gas periodically driven by finite-duration standing-wave laser pulses

Benjamin T. Beswick,[*] Ifan G. Hughes, and Simon A. Gardiner[†]

Joint Quantum Centre (JQC) Durham–Newcastle, Department of Physics, Durham University, Durham DH1 3LE, United Kingdom

Hippolyte P. A. G. Astier[‡]

Department of Physics, Cavendish Laboratory, Cambridge CB3 0HE, United Kingdom

Mikkel F. Andersen

Dodd–Walls Centre for Photonics and Quantum Technologies, Department of Physics, University of Otago, Dunedin 9016, New Zealand

Boris Daszuta

Department of Mathematics and Statistics, University of Otago, Dunedin 9054, New Zealand

Atom interferometers are a useful tool for precision measurements of fundamental physical phenomena, ranging from the local gravitational-field strength to the atomic fine-structure constant. In such experiments, it is desirable to implement a high-momentum-transfer "beam splitter," which may be achieved by inducing quantum resonance in a finite-temperature laser-driven atomic gas. We use Monte Carlo simulations to investigate these quantum resonances in the regime where the gas receives laser pulses of finite duration and derive an ϵ-classical model for the dynamics of the gas atoms which is capable of reproducing quantum resonant behavior for both zero-temperature and finite-temperature noninteracting gases. We show that this model agrees well with the fully quantum treatment of the system over a time scale set by the choice of experimental parameters. We also show that this model is capable of correctly treating the time-reversal mechanism necessary for implementing an interferometer with this physical configuration and that it explains an unexpected universality in the dynamics.

I. INTRODUCTION

Microkelvin-temperature cold-atom gases are a useful medium for atom-optical experiments, including atom interferometry [1]. For light-pulse atom interferometry experiments it is desirable to implement a high-momentum-transfer "beam splitter" [2–4], which can be realized by subjecting an atomic gas to a periodically pulsed optical standing wave. By tuning the period of the pulse sequence to a specific value known as the Talbot time, the phenomenon of *quantum resonance* can be exploited to coherently split the atomic population of the gas in momentum space using minimal laser power.

A dilute atomic gas receiving pulses of a "short" duration is well approximated by the atom-optical δ-kicked rotor Hamiltonian [5]. The atom-optical δ-kicked rotor has long been the subject of study in the field of quantum chaos [6,7], aided by the relative simplicity of both the classical and the quantum δ-kicked rotor. This includes the existence of some analytical results, as well as the ease with which the quantum δ-kicked rotor lends itself to Fourier methods [8,9]. Though laser pulses of a truly infinitesimal duration are clearly unachievable experimentally, this model successfully describes experiments where the distance traveled by the atomic center of mass during each pulse is negligible relative to the spatial period of the standing wave [10–29] (the so called

Raman-Nath regime [30]). However, experiments indicate that finite pulse-duration effects [31,32] can increase the sensitivity of atom interferometry experiments [33]. This consideration, coupled with the fact that the infinitesimal pulse approach gives erroneous predictions over larger time scales [34], motivates their incorporation into the kicked particle Hamiltonian. Though finite-duration-pulse atom interferometers have been investigated numerically for a single kicked particle [30], an investigation for a thermal gas of kicked particles is absent from the literature.

A possible reason for this absence is that simulating driven systems with finite-duration pulses is notably more numerically complex than simulating systems with δ kicks [30], and this problem scales substantially with the number of particles. Given that knowledge of how the momentum distribution changes over time is necessary for designing and operating light-pulse atom interferometry experiments, we are motivated to introduce a computationally simpler model, which can give accurate results for a typical experimental setup.

In this paper we introduce an ϵ-pseudoclassical model for the quantum kicked particle conceptually similar to that introduced by Fishman, Guarneri, and Rebbuzzini to describe quantum accelerator modes [35,36]. This model is attractive due to its mathematical simplicity and the minimal computational complexity of the numerics. We explore the predictions of this model using a Monte Carlo approach and compare the results to a fully quantum treatment. We find that the model captures the essential features of quantum resonant dynamics in finite-temperature driven gases. This is a model where the entire dynamics is described by ensembles of artificial classical

---
[*]b.t.beswick@durham.ac.uk
[†]s.a.gardiner@durham.ac.uk
[‡]hpaga2@cam.ac.uk

particles, which we find works remarkably well in modeling what is entirely a wave-interference phenomenon. We present an unexpected universality in the dynamics and find that the domain of validity of the model covers physically interesting parameters of direct experimental relevance.

The paper is organized as follows: in Sec. II we give an overview experimental considerations and describe the model system Hamiltonian and the time evolution it generates; in Sec. III we derive how to treat the existence of a finite-duration pulse (assuming that we are in the equivalent of a quantum-resonant regime for the δ-kicked rotor) using an ϵ-pseudoclassical model; in Sec. IV we describe the Monte Carlo methodologies we use to determine our numerical results; in Sec. V we compare and contrast numerical results using both full quantum dynamics and the pseudoclassical model; and in Sec. VI we present our conclusions.

II. SYSTEM OVERVIEW

A. Experimental considerations

As a typical system, one can consider a cloud of 10^5 cesium-133 atoms. This can be relatively straightforwardly confined and cooled in a magneto-optical trap, followed by an optical molasses, to a temperature of $\sim 5\,\mu$K. In this regime the resulting cold-atom gas is sufficiently dilute that atom-atom interactions can typically be neglected. Even lower temperatures can be achieved by Raman sideband cooling [39] or by cooling to quantum degeneracy [22,29]. (Inter-atomic interactions can be significant in a Bose-Einstein condensate, however, in principle, these can be substantially tuned away by exploiting an appropriate magnetic Feshbach resonance [40–44] or letting the cloud expand.)

The atomic cloud can then be released under gravity, while two counter-propagating laser beams of wavelength λ_L (choosing $\lambda_L = 852$ nm corresponds to the wavelength of the cesium D_2 transition) form a laser standing wave in the horizontal direction (see Fig. 1), which can be periodically pulsed [11–29,31,32]. By carefully tuning the phase-shifter element in Fig. 1, the laser beams will form a "walking wave," appearing as a standing wave in a frame comoving
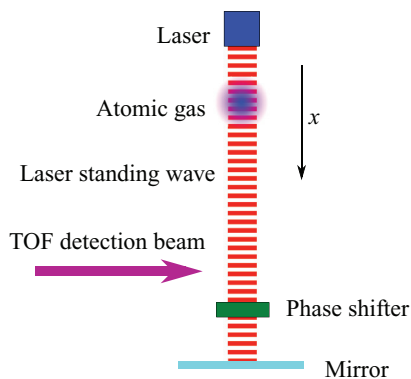

FIG. 1. Schematic of a possible experimental setup [37]. The time-of-flight (TOF) beam measures the atomic momentum distribution. If it is vertically oriented, the effect of the gravitational field can be transformed away [38] by use of the phase shifter element, for example, an electro-optic modulator [37].

with the local gravitational acceleration [37,38]. Neglecting interactions allows for a theoretical description using a single-particle Hamiltonian, which we describe in Sec. II B.

After receiving a set number of laser pulses, a time-of-flight measurement can be performed to determine the momentum distribution of the gas (and thence its momentum variance). These experimental observables are typically what one would measure in light-pulse atom interferometry experiments (see Sec. II D), and we explain how they may be predicted numerically in Sec. IV.

B. System Hamiltonian

During a laser pulse, the appropriate single-particle Hamiltonian describes a two-level atom (ground state $|g\rangle$ and excited state $|e\rangle$) of mass M coupled to a laser standing wave of angular frequency ω_L, wave number $k_L \equiv 2\pi/\lambda_L$, and phase ϕ [45,46],

$$\hat{H}_{2L} = \frac{\hbar\omega_0}{2}(|e\rangle\langle e| - |g\rangle\langle g|) + \frac{\hat{p}^2}{2M}$$
$$+ \frac{\hbar\Omega}{2}\cos(k_L\hat{x})[e^{-i(\omega_L t - \phi)}|e\rangle\langle g| + \text{H.c.}], \quad (1)$$

where Ω is the on-resonance Rabi frequency, t is the time, and H.c. stands for Hermitian conjugate. Here, $\hat{x}$ and $\hat{p}$ represent the atomic position and momentum along the axis of the laser standing wave [47]. Transforming to an appropriate rotating frame and adiabatically eliminating the excited state (assuming that the laser field is far detuned and that all population begins in the ground state also justifies our neglect of spontaneous emission) results in the Hamiltonian [45]

$$\hat{H}''_{2L} = \frac{\hat{p}^2}{2M} - \frac{\hbar\Omega^2}{8\Delta}\cos(2k_L\hat{x}), \quad (2)$$

where we have defined [48] $\Delta \equiv \omega_0 - \omega_L$. We describe the standing wave as being periodically switched on and off through the dimensionless time-dependent function $f(t)$, giving

$$\hat{H} = \frac{\hat{p}^2}{2M} - \hbar\phi_d\cos(K\hat{x})\frac{f(t)}{t_p}, \quad (3)$$

where we have introduced $K \equiv 2k_L$ and $\phi_d \equiv \Omega^2 t_p/8\Delta$. The function $f(t) = \sum_{n=-\infty}^{\infty} F_{\text{sq}}(t - nT, t_p)$, where

$$F_{\text{sq}}(t, t_p) = \begin{cases} 1 & \text{for} \quad 0 < t \leqslant t_p, \\ 0 & \text{for} \quad t \leqslant 0 \quad \text{or} \quad t > t_p \end{cases} \quad (4)$$

describes a square pulse of duration t_p. This is typically a reasonable description of atom optical experiments [18]. As $t_p \to 0$, then $f(t)/t_p \to \sum_{n=-\infty}^{\infty} \delta(t - nT)$, and in this limit Eq. (3) reduces to the familiar δ-kicked particle Hamiltonian described in [45].

C. Time evolution

The time periodicity of the Hamiltonian allows us to define a Floquet operator $\hat{F}$, such that $|\psi_{n+1}\rangle = \hat{F}|\psi_n\rangle$, where $|\psi_n\rangle$

denotes the state of the system immediately before the nth kick,

$$
\begin{aligned}
\hat{F} &= \hat{U}_{\text{Free}}\hat{U}_{\text{Kick}} \\
&= \exp\left(-i\frac{\hat{p}^2}{2M}\frac{[T-t_p]}{\hbar}\right) \\
&\quad\times \exp\left(-i\left[\frac{\hat{p}^2}{2M} - \frac{\hbar\phi_d}{t_p}\cos(K\hat{x})\right]\frac{t_p}{\hbar}\right),
\end{aligned}
\tag{5}
$$

where $\hat{U}_{\text{Free}}$ governs the "between-kick" free evolution, and $\hat{U}_{\text{Kick}}$ governs the time evolution while the kick is applied.

It is convenient to partition the position and momentum operators [50] such that

$$
K\hat{x} = 2\pi\hat{l} + \hat{\theta},
\tag{6a}
$$

$$
\hat{l}|Kx = 2\pi l + \theta\rangle = l|Kx = 2\pi l + \theta\rangle,
\tag{6b}
$$

$$
\hat{\theta}|Kx = 2\pi l + \theta\rangle = \theta|Kx = 2\pi l + \theta\rangle,
\tag{6c}
$$

where $l \in \mathbb{Z}$ and $\theta \in [0,2\pi)$ is effectively an angle variable, and

$$
(\hbar K)^{-1}\hat{p} = \hat{k} + \hat{\beta},
\tag{7a}
$$

$$
\hat{k}|(\hbar K)^{-1}p = k + \beta\rangle = k|(\hbar K)^{-1}p = k + \beta\rangle,
\tag{7b}
$$

$$
\hat{\beta}|(\hbar K)^{-1}p = k + \beta\rangle = \beta|(\hbar K)^{-1}p = k + \beta\rangle,
\tag{7c}
$$

with $k \in \mathbb{Z}$ and $\beta \in [-1/2,1/2)$. We can speak of k as the discrete part of the dimensionless momentum $(\hbar K)^{-1}p$ and of β as the continuous part or *quasimomentum*.

Fourier analysis of the Floquet operator $\hat{F}$ reveals that only momentum states separated by integer multiples of $\hbar K$ are coupled [13], and so β must be a conserved quantity; in other words, $[\hat{\beta},\hat{H}] = 0$ [11,50]. Within any specified quasimomentum subspace we can therefore consider the time evolution to be governed by

$$
\begin{aligned}
\hat{F}(\beta) &= \exp\left(-i\frac{[\hbar K(\hat{k}+\beta)]^2}{2M}\frac{[T-t_p]}{\hbar}\right) \\
&\quad\times \exp\left(-i\left\{\frac{[\hbar K(\hat{k}+\beta)]^2}{2M} - \frac{\hbar\phi_d}{t_p}\cos(\hat{\theta})\right\}\frac{t_p}{\hbar}\right).
\end{aligned}
\tag{8}
$$

We now have a continuum of Floquet operators, one for each β subspace, within which β can be considered simply a number [35,36,50]. For the most general time evolutions one should, in principle, take relative phases between these subspaces into account, however, this can be neglected if we do not consider coherent superpositions of states with different values of β.

D. Quantum resonance, antiresonance, and time reversal

For the δ-kicked rotor, quantum resonance occurs when the free evolution between kicks has no net effect on the state of the system [5,6,8,11,51,52]. Referring to Eq. (8) when $\beta = 0$ and $t_p \to 0$, this corresponds formally to requiring $\hat{U}_{\text{Free}}$ to collapse to the identity operator. Recalling that $\hat{k}$ has integer eigenvalues, this is fulfilled when

$$
T = T_T \equiv \frac{4\pi M}{\hbar K^2}
\tag{9}
$$

or any integer multiple thereof. The quantity T_T is known as the *Talbot time* [37,53], in analogy with the *Talbot length* of optics [54]. Within the $\beta = 0$ subspace (which maps exactly to the case of the quantum δ-kicked rotor, with its intrinsically discrete angular momentum spectrum), adjusting the period to an integer multiple of the Talbot time gives rise to an exactly quadratic increase in $\langle\hat{p}^2\rangle$ over time, given by $\langle\hat{p}^2\rangle_n = \hbar^2 K^2 \phi_d^2 n^2/2$ [52,55], where n is the number of kicks.

Assuming that the initial momentum distribution is symmetric about a mean value of 0, such ballistic growth of the system energy occurs via significant populations being transferred into high-magnitude momentum states of opposite value (leading, at low temperatures, to a distribution with large, negative *kurtosis* [52]). This splitting of the atomic momentum distribution can form the first component of a light-pulse atom interferometer [30,56], acting as the atom-optical analog of a beam splitter in classical optics. In an interferometric experiment, a relative phase would be accumulated between the "arms" of the resultant split cloud, due to coherent evolution caused by a perturbation being measured. At a time t_R, the laser standing wave can be near instantaneously phase-shifted in θ by an offset of π, which effectively reverses the quantum resonant dynamics and causes the momentum-state populations to recombine some time later. At this time the relative phase, and hence the magnitude of the perturbation, can be extracted.

For the case where the period T is set to a half-integer multiple of the Talbot time a phenomenon known as antiresonance can also be observed, characterized by kick-to-kick motion where there is no net increase in $\langle\hat{p}^2\rangle$ over time but, instead, $\langle\hat{p}^2\rangle$ alternates between two values [12,34,45,55].

III. TREATING FINITE-DURATION PULSES

A. Motivation for a pseudoclassical approach

In the Floquet operator for the quantum δ-kicked particle the position and momentum operators are explicitly separated, making numerical determination of the system time evolution straightforward. Incorporating finite-duration pulses combines $\hat{x}$ and $\hat{p}$ in the $\hat{U}_{\text{Kick}}$ operator of Eq. (5), substantially increasing the numerical task. We are therefore motivated to introduce a simpler treatment, based on ϵ-*pseudoclassics*, which is intended to approximate the fully quantum treatment in an appropriate regime; similar treatments can be found in [36], [50], and [57–59]. The evolution of a quantum particle or ensemble of quantum particles is modeled by a Monte Carlo simulation of an ensemble of pseudoclassical particles (described in Sec. IV), attractive due to both its computational simplicity and its dynamical insight.

B. Derivation of the pseudoclassical model

We begin with the Floquet operator corresponding to the kicked-particle Hamiltonian, restricted to a particular β subspace [Eq. (8)], together with the constraint $T = \ell T_T/2$ (where ℓ is an even integer: this corresponds to the condition for quantum resonance for the δ-kicked particle). Introducing the dimensionless pulse duration $\epsilon = \hbar K^2 t_p/M$, we may

rewrite Eq. (8) as

$$\hat{F}(\beta) = \exp\left(i\left[\frac{\hat{k}^2}{2}\epsilon + \hat{k}\beta(\epsilon - 2\pi\ell)\right]\right)$$

$$\times \exp\left(-i\left[\frac{\hat{k}^2}{2}\epsilon + \hat{k}\beta\epsilon - \phi_d\cos(\hat{\theta})\right]\right). \quad (10)$$

We now define a rescaled and shifted discrete momentum $\hat{\mathcal{J}}(\beta) = (\hat{k} + \beta)\epsilon$, leading to the commutator $[\hat{\theta}, \hat{\mathcal{J}}(\beta)] = i\epsilon$. Introducing the rescaled kicking strength $\tilde{V} = \epsilon\phi_d$, we can now rewrite Eq. (10) as

$$\hat{F}(\beta) = \exp\left(\frac{i}{\epsilon}\left[\frac{\hat{\mathcal{J}}(\beta)^2}{2} - \hat{\mathcal{J}}(\beta)2\pi\ell\beta\right]\right)$$

$$\times \exp\left(-\frac{i}{\epsilon}\left[\frac{\hat{\mathcal{J}}(\beta)^2}{2} - \tilde{V}\cos(\hat{\theta})\right]\right). \quad (11)$$

Note that ϵ appears where we would normally expect to see $\hbar$; for small values of ϵ, we therefore expect an effective classical model to give reasonable results which well approximate the quantum treatment [36,50,57–59].

The dynamics governed by Eq. (11) are equivalent to those generated by the following dimensionless Hamiltonians,

$$\hat{H}_1 = \frac{\hat{\mathcal{J}}(\beta)^2}{2} - \tilde{V}\cos(\hat{\theta}), \quad (12a)$$

$$\hat{H}_2 = -\frac{\hat{\mathcal{J}}(\beta)^2}{2} + \hat{\mathcal{J}}(\beta)2\pi\ell\beta, \quad (12b)$$

where $\hat{H}_1$ is associated with the kick and $\hat{H}_2$ with the free evolution, and each Hamiltonian governs the time evolution for 1 dimensionless time unit (rescaled time given by t/t_p). Replacing the quantum Hamiltonian $\hat{H}_1$ with its classical counterpart H_1, we determine Hamilton's equations of motion,

$$\dot{\theta}(\beta) = \frac{\partial H_1}{\partial \mathcal{J}(\beta)} = \mathcal{J}(\beta), \quad (13a)$$

$$\dot{\mathcal{J}}(\beta) = -\frac{\partial H_1}{\partial \theta(\beta)} = -\tilde{V}\sin[\theta(\beta)], \quad (13b)$$

which we recognize as the equations of motion of a simple pendulum, the phase-space orbits of which are, in principle, exactly solvable in terms of Jacobi elliptic functions (although they can be more convenient to solve numerically). Referring to a phase-space point immediately before the nth kick as $(\theta_n(\beta), \mathcal{J}_n(\beta))$, we say that evolving these values under Eq. (13) for 1 dimensionless time unit yields $(\theta_{n^+}(\beta), \mathcal{J}_{n^+}(\beta))$. Feeding these values into the classical equations of motion generated by H_2 yields the very simple classical map

$$\theta_{n+1}(\beta) = \theta_{n^+}(\beta) - \mathcal{J}_{n^+}(\beta) + 2\pi\ell\beta, \quad (14a)$$

$$\mathcal{J}_{n+1}(\beta) = \mathcal{J}_{n^+}(\beta), \quad (14b)$$

where $(\theta_{n+1}(\beta), \mathcal{J}_{n+1}(\beta))$ is the phase-space point evolved to just before the $(n+1)$th kick.

Finally, relating the dimensionless momentum $\mathcal{J}(\beta)$ back to the momentum p yields

$$p = \hbar K(k + \beta) = \frac{\hbar K}{\epsilon}\mathcal{J}(\beta). \quad (15)$$

To calculate the time evolution of expectation values using this treatment, we evolve an appropriate initial ensemble of classical particles and then compute their normalized statistics, as described below.

IV. MONTE CARLO SIMULATIONS

A. Quantum model

In our finite-temperature simulations, we follow the approach of Saunders *et al.* [45] and work within the momentum basis. The initial states are momentum eigenstates, with randomly distributed values sampled from the Maxwell-Boltzmann distribution,

$$D_k(\beta) = \frac{1}{w\sqrt{2\pi}}\exp\left(\frac{-[k+\beta]^2}{2w^2}\right), \quad (16)$$

where the temperature $\mathcal{T}_w = \hbar^2 K^2 w^2 / Mk_B$ [45].

Time-evolving an initial momentum eigenstate $|(\hbar K)^{-1}p = k + \beta\rangle$ using the Floquet operator $\hat{F}(\beta)$ of Eq. (10) results in a transfer of the initial population among other momentum eigenstates, such that the time-evolved state can be written $|\psi(t)\rangle_j = \sum_k c_{kj}(t)|(\hbar K)^{-1}p = k + \beta\rangle$, where $|\psi(t)\rangle_j$ is the time-evolved state corresponding to the jth of N_q initial momentum eigenstates. The second-order momentum moment is given by $\langle \hat{p}^2\rangle(t) = N_q^{-1}\sum_j\langle \hat{p}^2\rangle_j(t) = N_q^{-1}\sum_j\langle\psi(t)|_j\hat{p}^2|\psi(t)\rangle_j$. The momentum distribution can be read off from the absolute square of the coefficients $c_{kj}(t)$ for the case of a single initial momentum state and tells us the probability of the system's being in a given k subspace (some given value of k but any value of β). For an ensemble of N_q states, the total probability $P_k(t)$ of finding an atom with a certain discrete momentum k is given by the normalized sum of the absolute squares of the $c_{kj}(t)$ coefficients, $P_k = N_q^{-1}\sum_j|c_{kj}(t)|^2$.

It is desirable for our momentum distribution plots to be log-normalized so that fine features may be resolved. In practice, momentum states with higher k values receive a negligible amount of the population compared to states near $k = 0$, so when displaying our momentum distributions we impose a cutoff value C, such that the condition $P_k \geqslant C$ is true for all P_k and t and the problem of taking the logarithm of a near-zero population is avoided.

B. ϵ-pseudoclassical model

In the case of the ϵ-pseudoclassical model, momentum distribution dynamics are obtained by evolving a statistical ensemble of N_c classical particles according to Eq. (13) and Eq. (14) (note that N_c need not, in general, be equal to N_q). Though the trajectory of each particle does not in itself have a clear physical meaning, the evolution of an ensemble of sufficiently large size can be used to produce a facsimile of the quantum momentum-state population distribution of the gas. We place the momentum data into bins of width $\Delta p = \hbar K$,

normalize the resultant population distribution, and from this extract the mean squared momentum.

It is possible to produce an approximate momentum distribution also for the case of a zero-temperature gas, by setting $\mathcal{J}(\beta) = 0$ and choosing a random ensemble of initial θ values; the ensemble approximates a single momentum eigenstate with a given β. For the case of a finite-temperature gas, $\mathcal{J}(\beta)$ values are randomly drawn from a Maxwell-Boltzmann distribution, and θ values from a uniform distribution.

V. RESULTS

A. Dynamics of the pseudoclassical map

To gain insight into the system dynamics, it is useful to construct $(\theta, \mathcal{J})$ Poincaré sections, which in this case are stroboscopic maps defined by Eq. (13) and Eq. (14), evolved for some number of kicks N. We remark that we have opted to solve the equations of motion generated by H_1 numerically rather than using the exact Jacobi elliptic functions for ease of implementation; this still requires vastly less computational power to solve the time evolution of the system than the Fourier methods generally used in a fully quantum treatment. Inspection of Eq. (13) and Eq. (14) reveals that there are exactly two free parameters: the driving strength $\tilde{V}$ and the quasimomentum β. We therefore construct a selection of Poincaré sections varying these, choosing $\tilde{V} = 0.251$ when we vary β (Fig. 2; this value is motivated by typical experimental values [13,14,37,53,55,60–65]), and $\beta = 0$ when we vary $\tilde{V}$ (Fig. 3).

The Poincaré section in Fig. 2(a) [repeated in Fig. 3(a) for ease of comparison between different β subspaces and values of $\tilde{V}$] corresponds to that of an exact quantum resonance in the δ-kicked particle case (for which the dynamical behavior varies from resonant to antiresonant, depending on the value of β [38,45,52]). There are two stable fixed points visible, at (0,0) and $(-\pi,0) \equiv (\pi,0)$, each surrounded by concentric orbits
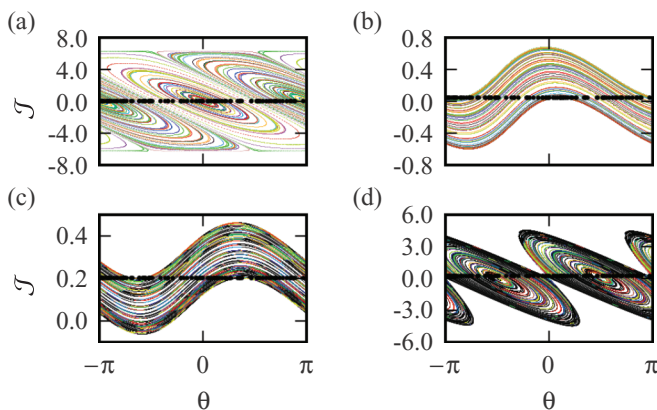

FIG. 2. Poincaré sections for $(\theta, \mathcal{J}(\beta))$ as evolved by Eq. (13) and Eq. (14), corresponding to the (a) $\beta = 0$, (b) $\beta = 0.05$, (c) $\beta = 0.2$, and (d) $\beta = 0.25$ subspaces, with $\ell = 2$ and $\tilde{V} = 0.251$. Each black circle represents one of 100 initial phase-space points, and each color represents the evolution of a single phase-space point over 1000 kicks. The smaller black points in (c) and (d) link up the rotational or elliptic orbits, respectively (which for $\beta = 0.2$ and $\beta = 0.25$, respectively, takes substantially longer than 1000 kicks).
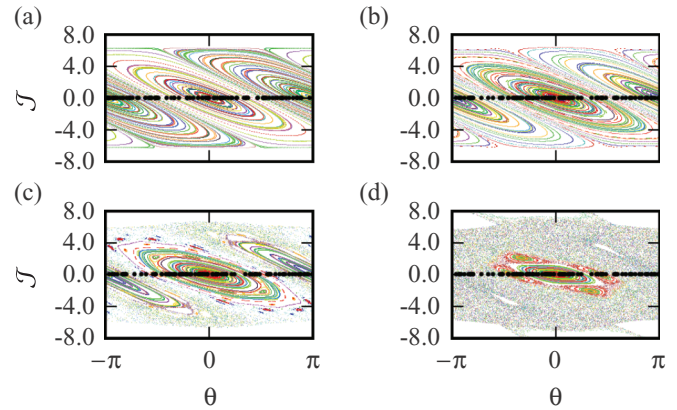

FIG. 3. Poincaré sections for $(\theta, \mathcal{J}(\beta))$ as evolved by Eq. (13) and Eq. (14), corresponding to the $\beta = 0$ subspace for driving strengths (a) $\tilde{V} = 0.251$, (b) $\tilde{V} = 2.51$, (c) $\tilde{V} = 5.01$, and (d) $\tilde{V} = 7.51$, with $\ell = 2$. Each black circle represents one of 100 initial phase-space points, and each color represents the evolution of a single phase-space point over 1000 kicks.

characteristic of regular (nonchaotic) motion. Figure 2(d) corresponds to the $\beta = 0.25$ subspace, which we expect to behave as an antiresonance in the δ-kicked limit. Clearly the system dynamics vary dramatically between different β subspaces, and we must therefore consider them all when modeling a thermal gas. We note that, although in our derivation of the pseudoclassical model we have assumed ℓ to be a positive even integer and β to be a real number between $-1/2$ and $1/2$, these only appear within the pseudoclassical model as $\ell\beta$, which can, in principle, take any real value. It is interesting to note that, as shown in Fig. 5(a), for $\ell = 2$ and $\beta = 0.25$ we see that the ϵ-pseudoclassical model also models quantum antiresonant behavior, primarily known in the context of the δ-kicked particle when $\beta = 0$ and $\ell = 1$ [45].

In Fig. 3 we see that, as we increase the driving strength $\tilde{V}$ from $\tilde{V} = 0.251$, a region of pseudorandom trajectories opens up in the outer parts of each system of elliptic orbits, until the Poincaré section becomes predominantly chaotic for $\tilde{V} = 7.51$. We remark that such high values of $\tilde{V}$, combined with small values of ϵ, correspond to very high laser intensities, making it unclear what the transition to chaos in the ϵ-pseudoclassical model really represents in an atom-optical context.

B. Zero-temperature gas

We now compute the evolution of $\langle \hat{p}^2 \rangle$ over time for a range of values of ϵ and constant ϕ_d (meaning that $\tilde{V} \equiv \epsilon\phi_d$ scales linearly with ϵ), using both the pseudoclassical and the fully quantum calculations, at zero temperature. This is actually computationally straightforward in the quantum case, as one need only evolve a single initial (zero momentum) eigenstate.

We display our results in Fig. 4(a). Two behaviors are clearly visible.

(1) As ϵ increases, the approximate pseudoclassical simulations deviate from the quantum dynamics after a smaller number of kicks. As this model relies on an expansion about ϵ as a smallness parameter, this deviation can be thought
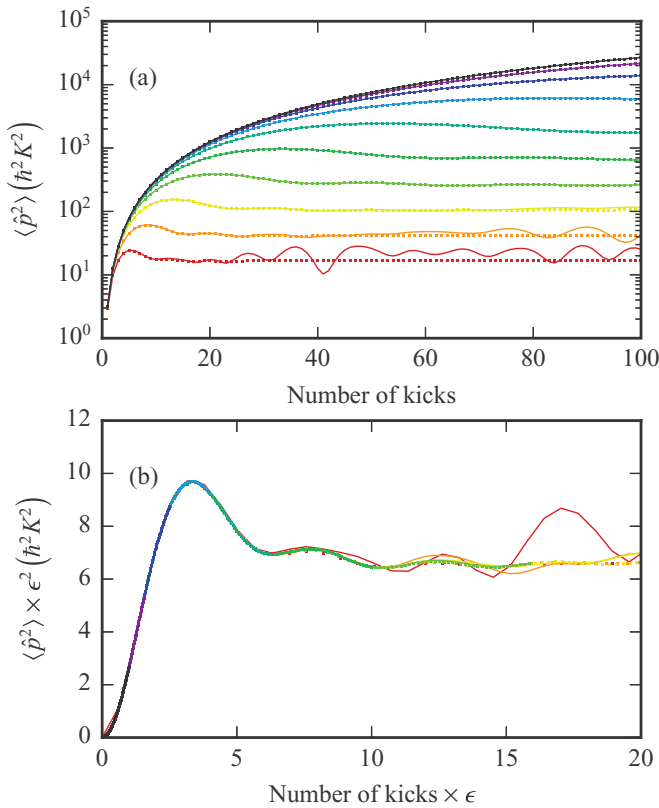
FIG. 4. (a) Plot of $\langle \hat{p}^2 \rangle$ in units of $\hbar^2 K^2$ vs number of kicks for a zero-temperature gas, with $\phi_d = 0.8\pi$ and $\ell = 2$. The scaled pulse duration ϵ takes the values $10^{-2+2j/10}$, where $j = \{0, 1, 2, \ldots, 9\}$. Curves represent the results of the quantum dynamics [Eq. (5)], and points those of the ϵ-pseudoclassical model [Eqs. (13) and (14)], with lower values of ϵ giving rise to higher peak values of $\langle \hat{p}^2 \rangle$. Hence, the uppermost curve (black) corresponds to $\epsilon = 0.01$ ($j = 0$) and the lowermost curve (red) to $\epsilon = 0.631$ ($j = 9$). (b) Rescaling of (a) by ϵ^2 on the $\langle \hat{p}^2 \rangle$ axis and ϵ on the kick-number axis such that a universal curve is revealed, where all data overlap over a suitably short time scale.

of as a cumulative error in the pseudoclassical dynamics that increases in magnitude each time the classical maps are applied. Results like those in Fig. 4(a) allow us to characterize time scales over which we can expect agreement between the pseudoclassical and the quantum treatments for a given value of ϵ.

(2) The peak value of $\langle \hat{p}^2 \rangle$ is higher for smaller values of ϵ. Recalling that ϵ is simply a rescaled pulse duration, as it approaches 0 the system behaves increasingly as if it were receiving δ kicks, for which $\langle \hat{p}^2 \rangle$ would increase indefinitely over time. It is again clear that the smaller the value of ϵ, the longer the time scale over which the system behaves as if it were δ kicked. At an ϵ-dependent point in time, $\langle \hat{p}^2 \rangle$ deviates from the quadratic growth associated with perfect quantum resonance, corresponding to violation of the Raman-Nath regime. We can see that $\langle \hat{p}^2 \rangle$ must eventually decrease by inspection of the phase-space diagram in Fig. 2(a), as the spread of trajectories is forced to eventually decrease simply because they manifest as bounded quasiperiodic orbits.

Rescaling the axes in Fig. 4(a) according to the value of ϵ reveals a universal curve, which exists independent

of this value, as displayed in Fig. 4(b). This universality appears to be essentially exact in the pseudoclassical model but ceases to apply for the quantum calculations once they deviate significantly from the pseudoclassical predictions. The observed oscillating decay encapsulates the dynamics visible in Fig. 2(a) and appears indicative of the dephasing of an ensemble of anharmonic oscillators. The time axis has been scaled by ϵ in order to make clear that we keep ϕ_d at a constant typical value as we scan the pulse duration. It should be noted, however, that the most natural axis scaling is by the parameter $\tilde{V} = \epsilon\phi_d$, as this is the only free parameter appearing explicitly in the ϵ-pseudoclassical model (for a given value of $\ell\beta$, which is $\ell\beta = 0$ in the case we consider here). In a sense this means that the true universal curve is more general, being preserved for all possible commensurate values of ϵ and ϕ_d in the range of $\tilde{V} = \epsilon\phi_d$ which we have explored in Fig. 4. The phase-space structures produced by Eq. (13) and Eq. (14) remain qualitatively the same over a wide range of values of $\tilde{V}$, as shown, for example, in Fig. 3(a) and Fig. 3(b). For the $\beta = 0$ case considered here, this means that essentially the same closed orbits are navigated, but at a rate which appears to be proportional to $\tilde{V}$. The equivalent values of $\tilde{V}$ used to generate the plots in Fig. 4 range from 0.251 [which is exactly the value used in Fig. 3(a)] to 1.65 [significantly less than the value of 2.51 used in Fig. 3(b)]. Identifying the maximum attainable value in the universal curve (or variants thereof, depending on which experimental parameters are varied) is potentially valuable in determining the largest attainable difference in momentum for the beam-splitting stage of an interferometer [33]. An example of this kind of procedure is found in [30], where a simple relationship to determine the optimal pulse duration emerged. Our better understanding of the scaling law, leading to universal curves such as that displayed in Fig. 4(b), means that a variety of parameters can be optimized according to quite general criteria.

Figure 5 shows comparisons of $\langle \hat{p}^2 \rangle$ evolution as computed by the quantum and ϵ-pseudoclassical models for initial conditions corresponding to a single momentum eigenstate with $k = 0$ and different values of β. The pseudoclassical and quantum models agree well over the entire range of β subspaces. Hence, for any reasonable initial momentum distribution, we can expect the pseudoclassical model to reproduce the correct quantum dynamics provided that ϵ is small enough on the time scale to be considered. We have chosen $\epsilon = 0.001$ for Fig. 5(a), where the dynamics are essentially coincident with those induced by perfect δ kicks for the chosen parameters and kick numbers. In Fig. 5(b) we have $\epsilon = 0.2$; comparing with Fig. 5(a) it is clear that the time evolution of $\langle \hat{p}^2 \rangle$ is significantly affected by the finite duration of the kicking pulses. Note, however, that although $\epsilon = 0.2$ would seem to be borderline in terms of being a "small parameter," the agreement between the ϵ-pseudoclassical model and the full quantum dynamics still appears to be excellent.

As β increases from 0 the evolution of $\langle \hat{p}^2 \rangle$ over time progresses from resonant to antiresonant behavior. This progression is twofold periodic in the space of quasimomenta: Eq. (14) shows that for $\ell = 2$ the same pseudoclassical dynamics are observed for $\beta + 1/2$ as for β (this symmetry can also be deduced for expectation values derived from the
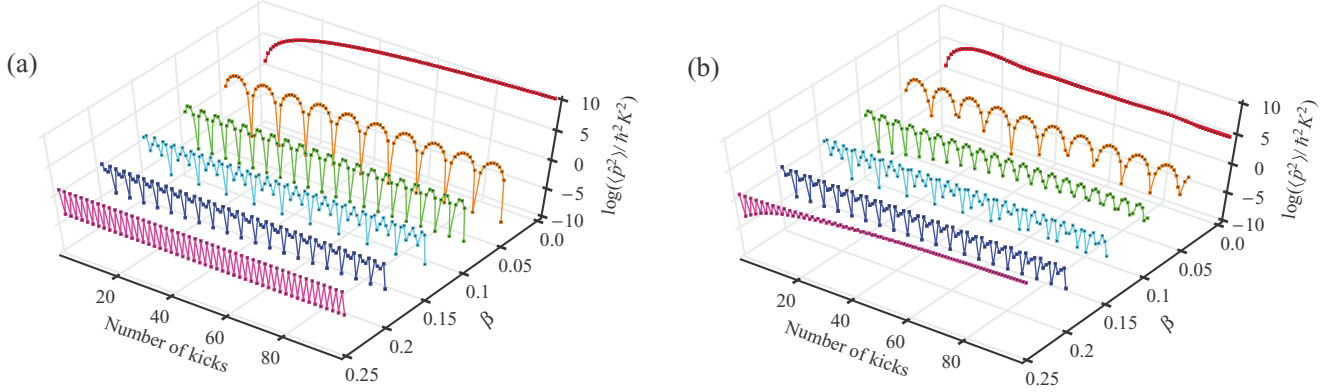
FIG. 5. Plots of the time evolution of the log of $\langle \hat{p}^2 \rangle$, in units of $\hbar^2 K^2$ vs number of kicks, for different values of the quasimomentum $\beta = \{0, 0.05, 0.1, 0.15, 0.2, 0.25\}$, for an otherwise zero-temperature gas [initial momentum eigenstate with $\mathcal{J}(\beta) = 0$]. Smooth curves represent results of the quantum evolution [Eq. (5)], and points those of the effective classical model [Eqs. (13) and (14)]. In (a) $\epsilon = 0.001$, and in (b) $\epsilon = 0.2$. Other parameters are $\phi_d = 0.8\pi$ and $\ell = 2$.

fully quantal Floquet operator [Eq. (11)] acting on momentum eigenstates [45]). Furthermore, the Hamiltonian is an even function of both $\hat{p}$ and $\hat{x}$, meaning that the same $\langle \hat{p}^2 \rangle$ dynamics are observed for $-\beta$ as for β. Hence, the data plotted in Fig. 5 effectively span the full range of β dependencies when the initial value of $\mathcal{J}(\beta)$ (or k) is equal to 0.

C. Finite-temperature Monte Carlo

We now perform comparative quantum and pseudoclassical Monte Carlo simulations for experimentally achievable time scales. The initial finite-temperature ensembles are chosen by random sampling from a Maxwell-Boltzmann distribution (combined with a uniform distribution for θ in the case
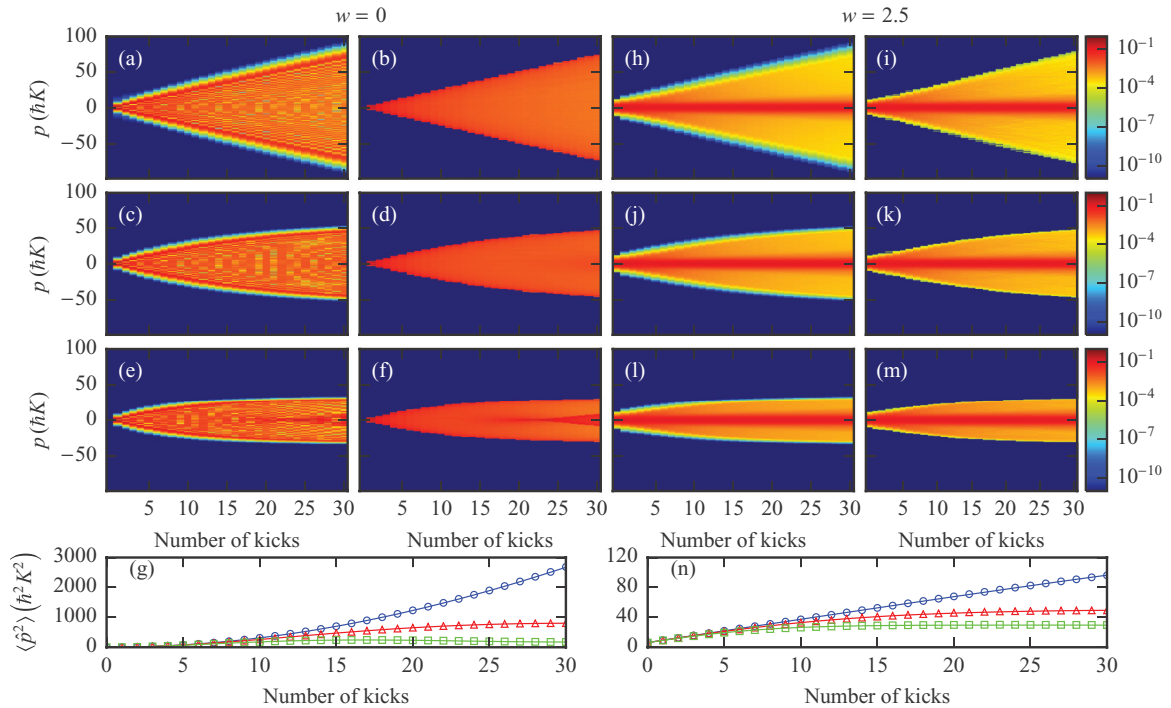

FIG. 6. Comparison of the dynamics of the momentum distributions computed by the fully quantum model [Eq. (5)] vs the pseudoclassical model [Eqs. (13) and (14)] for zero-temperature ($w = 0$) and finite-temperature ($w = 2.5$) gases, with $\phi_d = 0.8\pi$ and $\ell = 2$, for differing values of the scaled pulse duration ϵ. (a–f) Momentum distributions for a zero-temperature gas ($w = 0$) as computed by the quantum (a, c, e) and pseudoclassical (b, d, f) models. (h–m) Momentum distributions computed by the quantum (h, j, l) and effective classical (i, k, m) models, for $w = 2.5$. In each row, the distribution dynamics are computed for a different value of ϵ: for row 1 (a, b, h, i) $\epsilon = 0.02$, for row 2 (c, d, j, k) $\epsilon = 0.11$, and for row 3 (e, f, l, m) $\epsilon = 0.2$. To accommodate the logarithmic color scale, we have chosen a cutoff value of $C = 10^{-11}$. The corresponding time evolution of $\langle \hat{p}^2 \rangle$ (in units of $\hbar^2 K^2$) for (g) $w = 0$ and (n) $w = 2.5$; solid lines represent results of quantum calculations, and symbols results of the effective classical model (squares correspond to $\epsilon = 0.2$, triangles to $\epsilon = 0.11$, and circles to $\epsilon = 0.02$). Monte Carlo calculations were carried out with $N_c = 10^5$ particles, or $N_q = 10^5$ state vectors, as appropriate.

of the pseudoclassical dynamics), as described in Sec. IV. In Figs. 6(a)–6(f) and Figs. 6(h)–6(m), we compare the momentum distributions computed for three values of ϵ, using both the pseudoclassical and the quantum treatments, over a small number of kicks, at zero temperature ($w = 0$) and for cesium atoms at $\mathcal{T}_w \simeq 5$ μK ($w = 2.5$). In Fig. 6(g) and Fig. 6(n) we show the associated values of $\langle \hat{p}^2 \rangle$ computed for each case to check that our comparison takes place within the regime of validity of the ϵ-pseudoclassical model. For the zero-temperature ($w = 0$) case, the population splitting in momentum space characteristic of a quantum resonance can be seen in both models over the full 30 kicks for $\epsilon = 0.02$. For larger values of ϵ we observe a slowing in the momentum spreading, followed by a clear plateau in the case of $\epsilon = 0.2$, which is also visible in the corresponding plot of $\langle \hat{p}^2 \rangle$.

For each value of ϵ the overall shape of the momentum distribution computed by the ϵ-pseudoclassical model matches that of the fully quantum calculation well. A degree of internal structure is present in the zero-temperature ($w = 0$) quantum distributions that is not present in their ϵ-pseudoclassical counterparts. Similarly, in both the $w = 0$ and the $w = 2.5$ quantum distributions, there is further structure visible, where the most extreme populated states in momentum space meet the near-zero-population background, which is not present

in the pseudoclassical calculation. We can clearly see from Fig. 6(g) and Fig. 6(n) that the evolution of $\langle \hat{p}^2 \rangle$ is nonetheless reproduced perfectly over a short time scale. For the $w = 2.5$ case, we see a clearly defined feature centered around $p = 0$ representing a large concentration of the population. This is typical of finite-temperature quantum-resonant dynamics in atom-optical systems [10,34,45] and can be understood from Fig. 5; essentially a broad initial momentum distribution means that both resonant ($\beta = 0$) and bounded antiresonant ($\beta = 0.25$) dynamics take place simultaneously, as well as the whole range of intermediate behavior, leading to an overall averaging of the spreading in momentum space.

With atom interferometry in mind, we have repeated these simulations with the addition of a time-reversal event occurring at $n_R = 15$ kicks (as described in Sec. II D), and our results are displayed in Fig. 7. In Fig. 7(a) and Fig. 7(b) ($\epsilon = 0.02$ and $w = 0$) we clearly have a near-perfect time-reversal process, with the majority of the population returning to the zero-momentum state when $n = 2n_R$. Increasing ϵ to 0.11, we can see in Fig. 7(c) and Fig. 7(d) that the asymmetry about $n = 2n_R$ has increased very slightly, and for $\epsilon = 0.2$ we can see in Fig. 7(e) and Fig. 7(f) that the asymmetry has become even larger (similar effects were observed in [30]). For $w = 2.5$, however [Figs. 7(h)–7(n)], each distribution
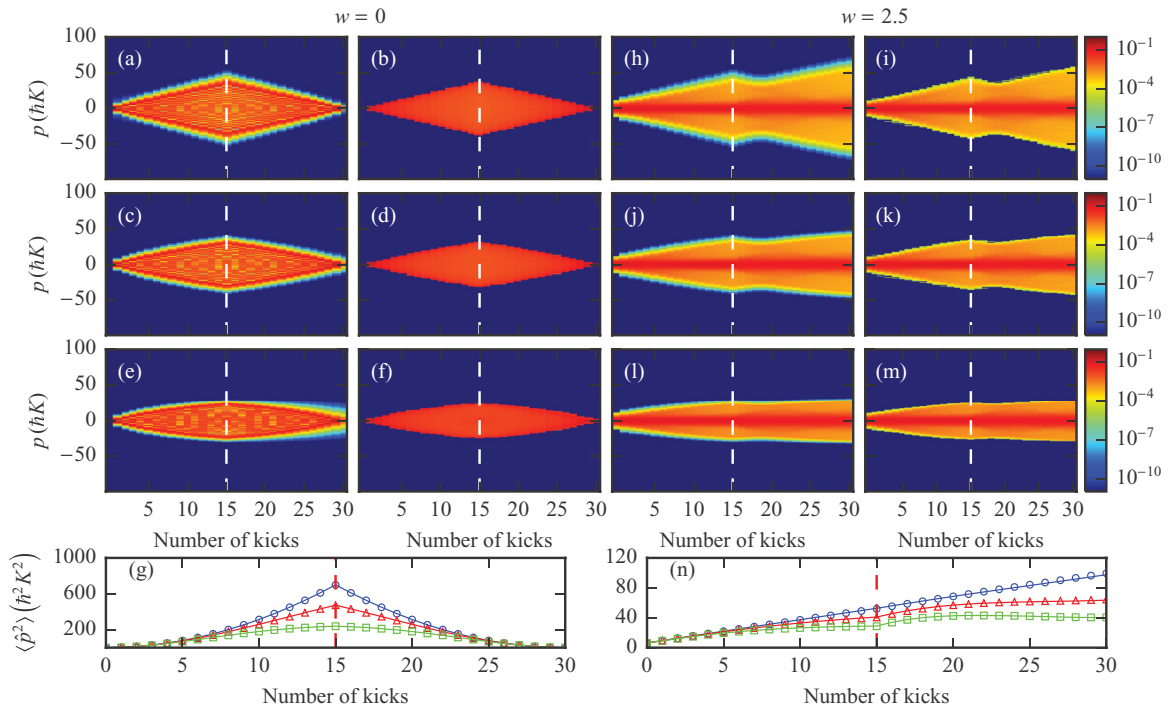

FIG. 7. Comparison of the dynamics of the momentum distributions computed by the fully quantum model [Eq. (5)] vs the pseudoclassical model [Eqs. (13) and (14)] for zero-temperature ($w = 0$) and finite-temperature ($w = 2.5$) gases, with $\phi_d = 0.8\pi$ and $\ell = 2$, for differing values of the scaled pulse duration ϵ. In each case a time-reversal event (phase-shifitng the standing wave by π) occurs at the 15th of 30 kicks (marked by the dashed lines). Momentum distributions for a zero-temperature gas ($w = 0$) as computed by (a, c, e) the quantum model and (b, d, f) the pseudoclassical model. Momentum distributions computed by (h, j, l) the quantum model and (i, k, m) the effective classical model, for $w = 2.5$. In each row, the distribution dynamics are computed for a different value of ϵ: for row 1 (a, b, h, i) $\epsilon = 0.02$, for row 2 (c, d, j, k) $\epsilon = 0.11$, and for row 3 (e, f, l, m) $\epsilon = 0.2$. To accommodate the logarithmic color scale, we have chosen a cutoff value of $C = 10^{-11}$. The corresponding time evolution of $\langle \hat{p}^2 \rangle$ [in units of $\hbar^2 K^2$] for (g) $w = 0$ and (n) $w = 2.5$; solid lines represent results of quantum calculations, and symbols results of the effective classical model (squares correspond to $\epsilon = 0.2$, triangles to $\epsilon = 0.11$, and circles to $\epsilon = 0.02$). Monte Carlo calculations were carried out with $N_c = 10^5$ particles, or $N_q = 10^5$ state vectors, as appropriate.
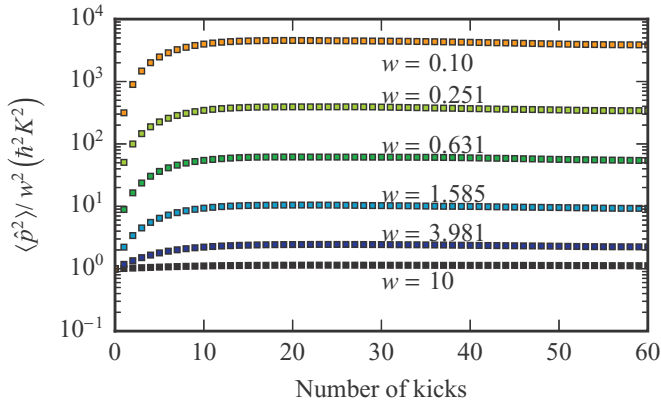
FIG. 8. Plots of the time evolution of $\langle \hat{p}^2 \rangle / w^2$ (in units of $\hbar^2 K^2$) vs the number of kicks, with $\epsilon = 0.2$, $\phi_d = 0.8\pi$, and $\ell = 2$. Each set of points corresponds to an individual value of $w = 10^{-1+2j/5}$, where $j = \{0, 1, 2, \ldots, 5\}$, as computed by the pseudoclassical model [Eqs. (13) and (14)].

begins to refocus but subsequently increases in breadth (this is the same behavior as expected for a δ-kicked atomic gas). Note that as the value of ϵ increases the final distributions become narrower, which is an effect of using finite-duration pulses.

In each case the ϵ-pseudoclassical predictions give good agreement with the shapes of the momentum distributions yielded by a fully quantum treatment, with the missing edge detail around each quantum distribution manifest only at around the $P_k = 10^{-7}$ level. Crucially, it is clear that the lack of internal structure in the ϵ-pseudoclassical distributions is not a problem for calculating $\langle \hat{p}^2 \rangle$ under time reversal or at a finite temperature. An interferometric measurement would look at deviations from a perfect time reversal, potentially motivating a study of the fidelity of a time-reversed kicked gas with finite-duration pulses, for example, using an approach similar to that derived for the δ-kicked rotor in [66].

Having carried out a detailed comparison of the quantum and ϵ-pseudoclassical models over relatively short time scales and at finite temperatures, we can reasonably assume that whatever value we select for w, the pseudoclassical model will produce accurate results, provided an appropriate value of ϵ is chosen. To better understand the variation of $\langle \hat{p}^2 \rangle$ with temperature over longer time scales, we have carried out simulations for six values of w, using only the ϵ-pseudoclassical model (results displayed in Fig. 8). We choose $\epsilon = 0.2$ for each simulation, as this is a relatively large value for which we have already shown excellent agreement of $\langle \hat{p}^2 \rangle$ with the fully quantum treatment over a range of 100 kicks (see Fig. 5). Plotting $\langle \hat{p}^2 \rangle / w^2$ versus the number of kicks n, the $n = 0$ value for each curve is the same, but from $n = 1$ they separate markedly: the lower the value of w, the greater the relative increase, due to the increased dominance of quantum-resonant behavior centered at $\beta = 0$. The dynamics of a single classical particle are generically simpler to compute than the evolution of a Schrödinger wave function, meaning that significant computational time can be saved in the physically relevant

case where it is necessary to propagate many individual wave functions to describe a thermal mixture.

VI. CONCLUSIONS

We have derived an ϵ-pseudoclassical model for quantum resonances in a finite-temperature dilute atomic gas driven by finite-duration off-resonant laser pulses and compared it to its fully quantum counterpart. The dynamics of the ϵ-pseudoclassical model have been investigated and certain phase-space features associated with quantum resonant behavior have been identified. Further, it has been shown that increasing the parameter ϵ shortens the time scale over which the quantum and ϵ-pseudoclassical calculations agree at zero temperature, as well as the amount of time before a quantum resonance begins to plateau due to violation of the Raman-Nath regime. The accuracy of the ϵ-pseudoclassical model has been shown to be unaffected by the initial state's quasimomentum and is, therefore, suitable for treating a finite-temperature gas. Monte Carlo simulations were explicitly performed to this end and compared both the expectation value $\langle \hat{p}^2 \rangle$ and the momentum distributions computed by each model, and it was found that the ϵ-pseudoclassical model reproduces the former essentially exactly, even at finite temperatures, and the general shape of the latter up to small details. We have also shown explicitly that the ϵ-pseudoclassical model correctly treats the time-reversal mechanism necessary for light-pulse atom interferometry. Finally, ϵ-pseudoclassical Monte Carlo simulations were performed to determine the behavior of $\langle \hat{p}^2 \rangle$ at different values of w for a large number of kicks. We expect this approach to be useful in quantifying the suitability of particular experimental parameter regimes for light-pulse atom interferometry.

The data presented in this paper are available. See Ref. [67].

APPENDIX: NUMERICAL METHODS

For every simulation using the ϵ-pseudoclassical model, Eq. (13) was integrated numerically using Adams' method, as implemented in the Python module *scipy.integrate.odeint*, which is based on the routine *lsoda*, from the FORTRAN library *odepack*. The integration time step in the interval between kicks was adaptively variable. Convergence was checked automatically and is also clearly indicated by the smooth nature of the phase-space trajectories observed in the nonchaotic regime. The map given by Eq. (14) was applied using simple matrix multiplication. For the quantum calculations, we employed a second-order split-step Fourier method, which we implemented in Python using the *numpy.fft.fft* and *numpy.fft.fftshift* routines. A total of 1000 split steps was used for each kicking pulse.

[1] A. Miffre, M. Jacquey, M. Büchner, G. Trénec, and J. Vigué, Atom interferometry, Phys. Scripta **74**, C15 (2006).

[2] P. Cladé, S. Guellati-Khélifa, F. Nez, and F. Biraben, Large Momentum Beam Splitter Using Bloch Oscillations, Phys. Rev. Lett. **102**, 240402 (2009).

[3] H. Müller, S. Chiow, S. Herrmann, and S. Chu, Atom Interferometers with Scalable Enclosed Area, Phys. Rev. Lett. **102**, 240403 (2009).

[4] S. Chiow, T. Kovachy, H.-C. Chien, and M. A. Kasevich, $102\hbar k$ Large Area Atom Interferometers, Phys. Rev. Lett. **107**, 130403 (2011).

[5] M. Saunders, Manifestation of quantum resonant effects in the atom-optical Delta-Kicked accelerator, Ph.D. thesis, University of Durham, UK, 2009.

[6] L. E. Reichl, *The Transition to Chaos* (Springer-Verlag, New York, 2004).

[7] A. J. Lichtenberg and M. A. Lieberman, *Regular and Chaotic Dynamics* (Springer-Verlag, New York, 1992).

[8] F. M. Izrailev and D. L. Shepelyanskii, Quantum resonance for a rotator in a nonlinear field, Theor. Math. Phys. **43**, 553 (1980).

[9] A. C. Doherty, K. M. D. Vant, G. H. Ball, N. Christensen, and R. Leonhardt, Momentum distributions for the quantum δ-kicked rotor with decoherence, J. Opt. B **2**, 605 (2000).

[10] F. L. Moore, J. C. Robinson, C. F. Bharucha, B. Sundaram, and M. G. Raizen, Atom Optics Realization of the Quantum δ-Kicked Rotor, Phys. Rev. Lett. **75**, 4598 (1995).

[11] M. Bienert, F. Haug, W. P. Schleich, and M. G. Raizen, Kicked rotor in Wigner phase space, Fortschr. Phys. **51**, 474 (2003).

[12] D. H. White, S. K. Ruddell, and M. D. Hoogerland, Phase noise in the delta kicked rotor: From quantum to classical, New J. Phys. **16**, 113039 (2014).

[13] M. B. d'Arcy, R. M. Godun, M. K. Oberthaler, G. S. Summy, K. Burnett, and S. A. Gardiner, Approaching classicality in quantum accelerator modes through decoherence, Phys. Rev. E **64**, 056233 (2001).

[14] M. B. d'Arcy, R. M. Godun, M. K. Oberthaler, D. Cassettari, and G. S. Summy, Quantum Enhancement of Momentum Diffusion in the Delta-Kicked Rotor, Phys. Rev. Lett. **87**, 074102 (2001).

[15] M. Sadgrove, A. Hilliard, T. Mullins, S. Parkins, and R. Leonhardt, Observation of robust quantum resonance peaks in an atom optics kicked rotor with amplitude noise, Phys. Rev. E **70**, 036217 (2004).

[16] C. F. Bharucha, J. C. Robinson, F. L. Moore, B. Sundaram, Q. Niu, and M. G. Raizen, Dynamical localization of ultracold sodium atoms, Phys. Rev. E **60**, 3881 (1999).

[17] F. L. Moore, J. C. Robinson, C. Bharucha, P. E. Williams, and M. G. Raizen, Observation of Dynamical Localization in Atomic Momentum Transfer: A New Testing Ground for Quantum Chaos, Phys. Rev. Lett. **73**, 2974 (1994).

[18] B. G. Klappauf, W. H. Oskay, D. A. Steck, and M. G. Raizen, Quantum chaos with cesium atoms: Pushing the boundaries, Physica D: Nonlin. Phenom. **131**, 78 (1999).

[19] W. H. Oskay, D. A. Steck, and M. G. Raizen, Timing noise effects on dynamical localization, Chaos Solitons Fractals **16**, 409 (2003).

[20] K. Vant, G. Ball, and N. Christensen, Momentum distributions for the quantum δ-kicked rotor with decoherence, Phys. Rev. E **61**, 5994 (2000).

[21] J. F. Kanem, S. Maneshi, M. Partlow, M. Spanner, and A. M. Steinberg, Observation of High-Order Quantum Resonances in the Kicked Rotor, Phys. Rev. Lett. **98**, 083004 (2007).

[22] G. J. Duffy, A. S. Mellish, K. J. Challis, and A. C. Wilson, Nonlinear atom-optical δ-kicked harmonic oscillator using a Bose-Einstein condensate, Phys. Rev. A **70**, 041602 (2004).

[23] G. Behinaein, V. Ramareddy, P. Ahmadi, and G. S. Summy, Exploring the Phase Space of the Quantum δ-Kicked Accelerator, Phys. Rev. Lett. **97**, 244101 (2006).

[24] C. Ryu, M. F. Andersen, A. Vaziri, M. B. d'Arcy, J. M. Grossman, K. Helmerson, and W. D. Phillips, High-Order Quantum Resonances Observed in a Periodically Kicked Bose-Einstein Condensate, Phys. Rev. Lett. **96**, 160403 (2006).

[25] P. Szriftgiser, J. Ringot, D. Delande, and J. C. Garreau, Observation of Sub-Fourier Resonances in a Quantum-Chaotic System, Phys. Rev. Lett. **89**, 224101 (2002).

[26] H. Ammann and N. Christensen, Mixing internal and external atomic dynamics in the kicked rotor, Phys. Rev. E **57**, 354 (1998).

[27] K. Vant, G. Ball, H. Ammann, and N. Christensen, Experimental evidence for the role of cantori as barriers in a quantum system, Phys. Rev. E **59**, 2846 (1999).

[28] M. E. K. Williams, M. P. Sadgrove, A. J. Daley, R. N. C. Gray, S. M. Tan, A. S. Parkins, N. Christensen, and R. Leonhardt, Measurements of diffusion resonances for the atom optics quantum kicked rotor, J. Opt. B **6**, 28 (2004).

[29] G. J. Duffy, S. Parkins, T. Müller, M. Sadgrove, R. Leonhardt, and A. C. Wilson, Experimental investigation of early-time diffusion in the quantum kicked rotor using a Bose-Einstein condensate, Phys. Rev. E **70**, 056206 (2004).

[30] B. Daszuta and M. F. Andersen, Atom interferometry using δ-kicked and finite-duration pulse sequences, Phys. Rev. A **86**, 043604 (2012).

[31] D. A. Steck, V. Milner, W. H. Oskay, and M. G. Raizen, Quantitative study of amplitude noise effects on dynamical localization, Phys. Rev. E **62**, 3461 (2000).

[32] V. Milner, D. A. Steck, W. H. Oskay, and M. G. Raizen, Recovery of classically chaotic behavior in a noise-driven quantum system, Phys. Rev. E **61**, 7223 (2000).

[33] M. F. Andersen and T. Sleator, Lattice Interferometer for Laser-Cooled Atoms, Phys. Rev. Lett. **103**, 070402 (2009).

[34] W. H. Oskay, D. A. Steck, V. Milner, B. G. Klappauf, and M. G. Raizen, Ballistic peaks at quantum resonance, Opt. Commun. **179**, 137 (2000).

[35] S. Fishman, I. Guarneri, and L. Rebuzzini, A theory for quantum accelerator modes in atom optics, J. Stat. Phys. **110**, 911 (2003).

[36] S. Fishman, I. Guarneri, and L. Rebuzzini, Stable Quantum Resonances in Atom Optics, Phys. Rev. Lett. **89**, 084101 (2002).

[37] R. M. Godun, M. B. d'Arcy, M. K. Oberthaler, G. S. Summy, and K. Burnett, Quantum accelerator modes: A tool for atom optics, Phys. Rev. A **62**, 013411 (2000).

[38] M. Saunders, P. L. Halkyard, S. A. Gardiner, and K. J. Challis, Fractional resonances in the atom-optical δ-kicked accelerator, Phys. Rev. A **79**, 023423 (2009).

[39] M. Kasevich and S. Chu, Laser Cooling Below a Photon Recoil with Three-Level Atoms, Phys. Rev. Lett. **69**, 1741 (1992).

[40] S. Inouye, M. R. Andrews, J. Stenger, H.-J. Miesner, D. M. Stamper-Kurn, and W. Ketterle, Observation of Feshbach resonances in a Bose-Einstein condensate, Nature **392**, 151 (1998).

[41] J. L. Roberts, N. R. Claussen, J. P. Burke, C. H. Greene, E. A. Cornell, and C. E. Wieman, Resonant Magnetic Field Control of Elastic Scattering in Cold ^{85}Rb, Phys. Rev. Lett. **81**, 5109 (1998).

[42] T. Köhler, K. Góral, and P. S. Julienne, Production of cold molecules via magnetically tunable Feshbach resonances, Rev. Mod. Phys. **78**, 1311 (2006).

[43] M. Gustavsson, E. Haller, M. J. Mark, J. G. Danzl, G. Rojas-Kopeinig, and H.-C. Nägerl, Control of Interaction-Induced Dephasing of Bloch Oscillations, Phys. Rev. Lett. **100**, 080404 (2008).

[44] P. K. Molony, P. D. Gregory, Z. Ji, B. Lu, M. P. Köppinger, C. R. Le Sueur, C. L. Blackley, J. M. Hutson, and S. L. Cornish, Creation of Ultracold ^{87}Rb ^{133}Cs Molecules in the Rovibrational Ground State, Phys. Rev. Lett. **113**, 255301 (2014).

[45] M. Saunders, P. L. Halkyard, K. J. Challis, and S. A. Gardiner, Manifestation of quantum resonances and antiresonances in a finite-temperature dilute atomic gas, Phys. Rev. A **76**, 043415 (2007).

[46] Y. Zheng, Chaos and momentum diffusion of the classical and quantum kicked rotor, Ph.D. thesis, University of North Texas, 2005.

[47] We may consider the center-of-mass dynamics in the x direction in isolation, as they separate from the remaining center-of-mass degrees of freedom.

[48] Note that the detuning is usually defined as equal to $\omega_L - \omega_0$ [49] and thus is equal to $-\Delta$ as defined in this paper. Within the context of atom-optical δ-kicked rotors the convention used in this paper is typical, however [10,17].

[49] C. J. Foot, *Atomic Physics (Oxford Master Series in Atomic, Optical and Laser Physics)*, 1st ed. (Oxford University Press, New York, 2005).

[50] R. Bach, K. Burnett, M. B. d'Arcy, and S. A. Gardiner, Quantum-mechanical cumulant dynamics near stable periodic orbits in phase space: Application to the classical-like dynamics of quantum accelerator modes, Phys. Rev. A **71**, 033417 (2005).

[51] R. Lima and D. Shepelyansky, Fast Delocalization in a Model of Quantum Kicked Rotator, Phys. Rev. Lett. **67**, 1377 (1991).

[52] P. L. Halkyard, M. Saunders, S. A. Gardiner, and K. J. Challis, Power-law behavior in the quantum-resonant evolution of the δ-kicked accelerator, Phys. Rev. A **78**, 063401 (2008).

[53] M. K. Oberthaler, R. M. Godun, M. B. d'Arcy, G. S. Summy, and K. Burnett, Observation of Quantum Accelerator Modes, Phys. Rev. Lett. **83**, 4447 (1999).

[54] E. Hecht, *Optics* (Addison Wesley, San Francisco, 2002).

[55] A. Ullah, Delta-Kicked rotor experiments with an all-optical BEC, Ph.D. thesis, University of Auckland, 2012.

[56] A. D. Cronin, J. Schmiedmayer, and D. E. Pritchard, Optics and interferometry with atoms and molecules, Rev. Mod. Phys. **81**, 1051 (2009).

[57] C. F. Bharucha, Experiments in dynamical localization of ultracold sodium atoms using time-dependent optical potentials, Ph.D. thesis, The University of Texas at Austin, 1997.

[58] S. Wimberger, I. Guarneri, and S. Fishman, Quantum resonances and decoherence for δ-kicked atoms, Nonlinearity **16**, 1381 (2003).

[59] S. Wimberger, I. Guarneri, and S. Fishman, Classical Scaling Theory of Quantum Resonances, Phys. Rev. Lett. **92**, 084102 (2004).

[60] L. Rebuzzini, S. Wimberger, and R. Artuso, Delocalized and resonant quantum transport in nonlinear generalizations of the kicked rotor model, Phys. Rev. E **71**, 036220 (2005).

[61] S. Schlunk, M. B. d'Arcy, S. A. Gardiner, D. Cassettari, R. M. Godun, and G. S. Summy, Signatures of Quantum Stability in a Classically Chaotic System, Phys. Rev. Lett. **90**, 054101 (2003).

[62] S. Schlunk, M. B. d'Arcy, S. A. Gardiner, and G. S. Summy, Experimental Observation of High-Order Quantum Accelerator Modes, Phys. Rev. Lett. **90**, 124102 (2003).

[63] Z. Y. Ma, M. B. d'Arcy, and S. A. Gardiner, Gravity-Sensitive Quantum Dynamics in Cold Atoms, Phys. Rev. Lett. **93**, 164101 (2004).

[64] A. Buchleitner, M. B. d'Arcy, S. Fishman, S. A. Gardiner, I. Guarneri, Z.-Y. Ma, L. Rebuzzini, and G. S. Summy, Quantum Accelerator Modes from the Farey Tree, Phys. Rev. Lett. **96**, 164101 (2006).

[65] M. B. d'Arcy, R. M. Godun, D. Cassettari, and G. S. Summy, Accelerator-mode-based technique for studying quantum chaos, Phys. Rev. A **67**, 023605 (2003).

[66] M. Abb, I. Guarneri, and S. Wimberger, Pseudoclassical theory for fidelity of nearly resonant quantum rotors, Phys. Rev. E **80**, 035206(R) (2009).

[67] Data are available through Durham University data management at https://collections.durham.ac.uk/collections/ht24wj427.